Crystal and Magnetic Structures of $Ca_4Mn_3O_{10}$, an $n = 3$ Ruddlesden−Popper Compound

P. D. Battle,* M. A. Green, J. Lago, J. E. Millburn, M. J. Rosseinsky,* and J. F. Vente

Inorganic Chemistry Laboratory, University of Oxford, South Parks Road, Oxford OX1 3QR, U.K.

Received September 25, 1997. Revised Manuscript Received November 13, 1997

The crystal and magnetic structures of the $n = 3$ Ruddlesden−Popper phase with the ideal composition $Ca_4Mn_3O_{10}$ have been studied using X-ray and neutron powder diffraction. The crystal structure at 293 K is relatively insensitive to the partial pressure of oxygen used in sample preparation. A sample prepared in air showed an orthorhombic distortion (space group *Pbca*, $a = 5.26557(12)$, $b = 5.26039(11)$, $c = 26.8276(5)$ Å) from the ideal $n = 3$ RP structure, as did a sample prepared under 800 atm of O_2 pressure ($a = 5.26005(4)$, $b = 5.25569(4)$, $c = 26.83543(20)$ Å). Both samples showed a magnetic phase transition at 115 K from a paramagnetic phase with extensive short-range spin ordering to a weakly ferromagnetic ($\mu_{ferro} = 2 \times 10^{-3}\ \mu_B$ per Mn) low-temperature phase. The antiferromagnetic components of the atomic magnetic moments (2.23(2) μ_B per Mn) order in a G-type manner within each perovskite block, and the interblock coupling reflects the orthorhombic symmetry of the structure.

Introduction

Compounds of manganese have played a central role in recent studies of the magnetotransport properties of mixed metal oxides. It has been shown that the electrical resistivity of oxides containing Mn in a non-integral oxidation state ($Mn^{3+/4+}$) can decrease dramatically in an applied magnetic field, an observation that may lead to applications in the area of data storage. The effect has been most widely studied[1,2] in perovskites of the general form $Ln_{1-x}A_xMnO_3$, where the presence of both lanthanide (Ln) and alkaline earth (A) cations results in the adoption of a mixed-valence state by the Mn cation. Perovskite can be regarded as the $n = \infty$ member of the Ruddlesden−Popper (RP)[3] family of compounds $(Ln,A)_{n+1}B_nO_{3n+1}$, with the K_2NiF_4 structure being at the opposite ($n = 1$) extreme. RP phases can be considered to consist of perovskite-like blocks of vertex-sharing BO_6 octahedra which extend to infinity in the *xy* plane and have a thickness of *n* octahedra parallel to the *z* axis; neighboring blocks are separated by a rock-salt layer such that the overall composition can be described as $((Ln,A)BO_3)_n(Ln,A)O$. Following the observation of colossal magnetoresistance (CMR) in $n = \infty$ RP phases, the electronic properties of other members of the series have been studied. CMR is not observed in samples of the $n = 1$ system $Sr_{2-x}La_xMnO_4$ which, for $x \sim 0.5$, show charge ordering on the Mn sublattice.[4−7] However, CMR has been detected around the Curie temperature (126 K)[8] of the $n = 2$ composition $Sr_{1.8}La_{1.2}Mn_2O_7$, which does not show charge ordering. The majority of the data collected to date for $n = 1$, 2, and ∞ suggest that CMR is incompatible with charge ordering on the Mn sublattice and that it is closely linked to the appearance of a spontaneous magnetization in the sample. There are, however, a number of exceptions to this sweeping generalization. $Sr_{2-x}Nd_{1+x}Mn_2O_7$, for example, shows[9,10] CMR in the absence of a spontaneous magnetization. Studies of this system have demonstrated that the nature and behavior of the sample are very sensitive to the conditions used in the chemical synthesis.[11] The difference between the Nd- and La-containing $n = 2$ compounds demonstrates that the electronic properties are very sensitive to elemental composition, and diffraction experiments[12−14] have indicated that the sensitivity can be traced to the subtle

(1) Urushibara, A.; Moritomo, Y.; Arima, T.; Asamitsu, A.; Kido, G.; Tokura, Y. *Phys. Rev. B* **1995**, *51*, 14103.
(2) Rao, C. N. R.; Cheetham, A. K.; Mahesh, R. *Chem. Mater.* **1996**, *8*, 2421.
(3) Ruddlesden, S. N.; Popper, P. *Acta Crystallogr.* **1958**, *11*, 541.
(4) Bao, W.; Chen, C. H.; Carter, S. A.; Cheong, S.-W. *Solid State Commun.* **1996**, *98*, 55.
(5) Bouloux, J. C.; Soubeyroux, J. L.; Daoudi, A.; Flem, G. L. *Mater. Res. Bull.* **1981**, *16*, 855.
(6) Moritomo, Y.; Tomioka, Y.; Asamitsu, A.; Tokura, Y. *Phys Rev. B* **1995**, *51*, 3297.
(7) Sternlieb, B. J.; Hill, J. P.; Wildgruber, U. C.; Luke, G. M.; Nachumi, B.; Moritomo, Y.; Tokura, Y. *Phys. Rev. Lett.* **1996**, *76*, 2169.
(8) Moritomo, Y.; Asamitsu, A.; Kuwahara, H.; Tokura, Y. *Nature* **1996**, *380*, 141.
(9) Battle, P. D.; Blundell, S. J.; Green, M. A.; Hayes, W.; Honold, M.; Klehe, A. K.; Laskey, N. S.; Millburn, J. E.; Murphy, L.; Rosseinsky, M. J.; Samarin, N. A.; Singleton, J.; Sluchanko, N. A.; Sullivan, S. P.; Vente, J. F. *J. Phys.: Condensed Matter* **1996**, *8*, L427.
(10) Seshadri, R.; Martin, C.; Maignan, A.; Hervieu, M.; Raveau, B.; Rao, C. N. R. *J. Mater. Chem.* **1996**, *6*, 1585.
(11) Battle, P. D.; Hepburn, J.; Millburn, J. E.; Radaelli, P. G.; Rosseinsky, M. J.; Spring, L. E.; Vente, J. F. *Chem. Mater.* **1997**, *9*, 3215.
(12) Battle, P. D.; Green, M. A.; Laskey, N. S.; Millburn, J. E.; Radaelli, P.; Rosseinsky, M. J.; Sullivan, S. P.; Vente, J. F. *Phys. Rev. B* **1996**, *54*, 15967.
(13) Battle, P. D.; Cox, D. E.; Green, M. A.; Millburn, J. E.; Spring, L. E.; Radaelli, P. G.; Rosseinsky, M. J.; Vente, J. F. *Chem. Mater.* **1997**, *9*, 1042.
(14) Mitchell, J. F.; Argyriou, D. N.; Jorgensen, J. D.; Hinks, D. G.; Potter, C. P.; Bader, S. D. *Phys. Rev. B* **1997**, *55*, 63.

S0897-4756(97)00647-9 CCC: $15.00
Published on Web 01/06/1998

structural changes that are brought about by the variations in composition. The wide range of properties seen in the RP phases referred to above has prompted both ourselves and others to study the $n = 3$ phases, and magnetoresistance has recently been reported[15] in thin films containing $La_{2.1}Ca_{1.9}Mn_3O_{10}$. As formulated, $Ca_4Mn_3O_{10}$ is an oxide of Mn(IV), and it might therefore not be expected to show interesting magnetotransport properties. However, the most remarkable exception to the description of CMR given above involves the pyrochlore $Tl_2Mn_2O_7$ that shows the effect[16,17] close to the Curie temperature despite the fact that no mixed valency is present, at least within the sensitivity of the analysis techniques used to date.[18] We have therefore prepared $Ca_4Mn_3O_{10-\delta}$ under a range of oxygen pressures in an attempt to produce both fully oxidized and partially reduced samples. In the present paper we discuss the influence of synthesis conditions on the stoichiometry of the product, and we describe the crystal and magnetic structures of one representative sample; a detailed account of the electronic properties of $Ca_4Mn_3O_{10-\delta}$ will be given in a later publication.

Experimental Section

Polycrystalline samples of $Ca_4Mn_3O_{10-\delta}$ were prepared by reacting well-ground stoichiometric mixtures of $CaCO_3$ and MnO_2 under a variety of conditions. All preparations began with a relatively low-temperature heating sequence in air (typically 1 day at 800 °C, 1 day at 1000 °C, 2 days at 1200 °C) which initiated the reaction between the starting materials. It was necessary to use higher temperatures in order to produce pure samples of the $n = 3$ phase. One such sample (P) was synthesized after further firings in air at 1310 °C (27 h) and 1330 °C (four firings, 27 h), and then under 1 atm of flowing oxygen at 1330 °C (three firings, 27−33 h). A second sample (Q) was treated in air at 1300 °C (three days) and 1350 °C (six days), then under oxygen at 1310 °C (two days) and, finally, at 500 °C under 800 atm of O_2 pressure (6 days); this strategy was based on that used in an earlier synthesis of $Ca_4Mn_3O_{9.96}$.[19] Sample Q was cooled to room temperature at a rate of 10 °C min^{-1} while still under pressure. The highest temperature used in these reactions is close to the melting point of the product.

The purity of the products was established using X-ray powder diffraction data collected on a Siemens D5000 diffractometer operating with Cu $K\alpha_1$ radiation, and attempts were made to determine their oxygen content by iodometric titrations and thermogravimetric analysis. The magnetic susceptibilities of samples contained in gelatin capsules were determined in the temperature range $5 \le T/K < 300$ using a Quantum Design MPMS SQUID magnetometer. Data were collected after cooling the sample in the absence of an applied magnetic field (ZFC) and after cooling in the measuring field (FC). The diffractometer 2.3 at SRS, Daresbury Laboratory was used to collect high-resolution X-ray diffraction data ($\lambda = 1.3997$ Å) on the relatively small quantity of sample Q produced in the high-pressure synthesis. The larger quantities of sample P produced at ambient pressure were suitable for study by neutron diffraction. Data were collected at room temperature on the constant wavelength ($\lambda = 1.5943$ Å, $5 \le 2\theta/° \le 150$, $\Delta 2\theta = 0.05°$) diffractometer D2b at ILL, Grenoble, and at 5 K on the time-of-flight diffractometer IRIS ($2.1 \le d/Å < 5.5$) at Rutherford Laboratory. A diffraction pattern was also collected at room temperature on the HRPD diffractometer at Rutherford Laboratory. All powder diffraction data were analyzed by the Rietveld method,[20] using the GSAS[21] software package.

Table 1. Structural Parameters of $Ca_4Mn_3O_{10}$ (Sample Q) at 293 K[a]

atom	site	*x*	*y*	*z*
Ca(1)	8c	0.502(1)	0.480(1)	0.0694(2)
Ca(2)	8c	−0.015(1)	0.026(1)	0.2052(1)
Mn(1)	4b	0	$^1/_2$	0
Mn(2)	8c	0.491(1)	0.007(1)	0.14123(8)
O(1)	8c	0.422(2)	0.026(3)	0.0690(5)
O(2)	8c	0.532(3)	0.013(3)	0.2136(3)
O(3)	8c	0.778(4)	0.235(4)	0.1364(5)
O(4)	8c	0.219(4)	0.782(4)	0.1450(5)
O(5)	8c	0.289(5)	0.284(5)	−0.0068(6)

[a] One overall $U_{iso} = 0.0052(3)$ Å^2. Space group: *Pbca*. $a = 5.26005(4)$; $b = 5.25569(4)$; $c = 26.83543(20)$; $V = 741.869(10)$. Agreement indexes: $R_{wp} = 3.28\%$; $R_p = 2.31\%$; $R_f = 14.03$; $DWd = 0.953$; $\chi_{red}^2 = 2.54$ for 46 variables; cf. $I4/mmm$. $R_{wp} = 4.35\%$; $R_p = 2.76\%$; $R_f = 14.90$; $DWd = 0.634$; $\chi_{red}^2 = 4.44$ for 27 variables.

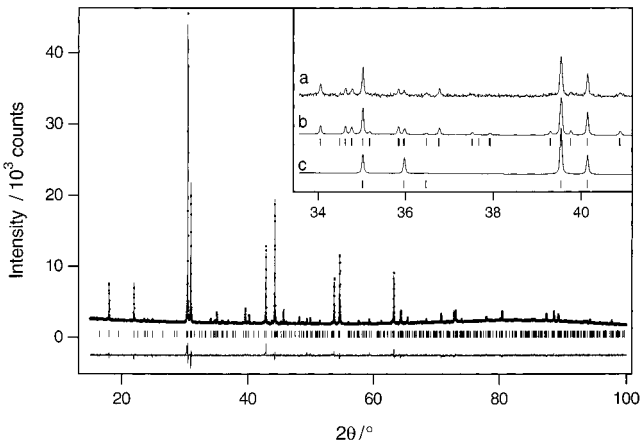

Figure 1. Observed, calculated, and difference X-ray diffraction profiles of $Ca_4Mn_3O_{10}$ (sample Q, prepared under 800 atm of O_2). Reflection positions are marked. The inset shows, for a limited angular region, (a) the observed pattern, (b) the fitted pattern in *Pbca*, and (c) the fitted pattern in $I4/mmm$

Results

The in-house X-ray diffraction patterns of the products P and Q indicated that both were single-phase samples of the tetragonal $n = 3$ RP phase $Ca_4Mn_3O_{10-\delta}$. However, we were unable to obtain a self-consistent chemical analysis, and we must therefore rely on the high-resolution diffraction data described below in order to establish the composition of our samples. The crystal structure of sample Q was refined from synchrotron X-ray powder diffraction data. In contrast to that collected in our own laboratory, this diffraction pattern could not be accounted for in the most likely tetragonal space group ($I4/mmm$) and an enlarged, orthorhombic unit cell (space group *Pbca*) was adopted in order to achieve a satisfactory refinement. A similar symmetry

(15) Asano, H.; Hayakawa, J.; Matsui, M. *Appl. Phys. Lett.* **1997**, *71*, 844.
(16) Shimakawa, Y.; Kubo, Y.; Manako, T. *Nature* **1996**, *379*, 53.
(17) Subramanian, M. A.; Toby, B. H.; Ramirez, A. P.; Marshall, W. J.; Sleight, A. W.; Kwei, G. H. *Science* **1996**, *273*, 81.
(18) Rosenfeld, H. D.; Subramanian, M. A. *J. Solid State Chem.* **1996**, *125*, 278.
(19) MacChesney, J. B.; Williams, H. J.; Potter, J. F.; Sherwood, R. C. *Phys. Rev.* **1967**, *164*, 779.
(20) Rietveld, H. M. *J. Appl. Crystallogr.* **1969**, *2*, 65.
(21) Larson, A. C.; von Dreele, R. B. General Structure Analysis System (GSAS), *Los Alamos National Laboratories*, Report LAUR 86-748, 1990.

Table 2. Selected Bond Distances (Å) and Angles (deg) for $Ca_4Mn_3O_{10}$ (Sample Q) at 293 K[a]

Ca(1)−O(1)^{i}	2.90(1)	Ca(2)−Mn(2)	3.058(7)	Mn(1)−O(1)	1.90(1) × 2
Ca(1)−O(1)^{ii}	2.42(1)			Mn(1)−O(5)$^{i/iii}$	1.90(3) × 2
Ca(1)−O(1)^{iii}	2.24(1)			Mn(1)−O(5)$^{ii/iv}$	1.87(3) × 2
Ca(1)−O(1)^{iv}	3.04(1)	Ca(2)−O(2)^{i}	2.39(1)		
Ca(1)−O(3)^{i}	2.64(1)	Ca(2)−O(2)^{ii}	2.89(1)	Mn(2)−O(1)	1.97(1)
Ca(1)−O(3)^{ii}	2.52(1)	Ca(2)−O(2)^{iii}	2.56(1)	Mn(2)−O(2)	1.95(1)
Ca(1)−O(4)^{i}	2.97(1)	Ca(2)−O(2)^{iv}	2.70(1)	Mn(2)−O(3)	1.93(2)
Ca(1)−O(4)^{ii}	2.56(1)	Ca(2)−O(2)^{v}	2.19(1)	Mn(2)−O(3)	1.88(2)
Ca(1)−O(5)^{i}	2.55(1)	Ca(2)−O(3)^{i}	2.40(1)	Mn(2)−O(4)	1.85(2)
Ca(1)−O(5)^{ii}	3.01(1)	Ca(2)−O(3)^{ii}	2.70(1)	Mn(2)−O(4)	1.82(2)
Ca(1)−O(5)^{iii}	2.36(1)	Ca(2)−O(4)^{i}	2.40(1)		
Ca(1)−O(5)^{iv}	2.64(1)	Ca(2)−O(4)^{ii}	2.61(1)	O(1)−O(5)	2.54(2)

[a] Superscripts relate to Figure 9.

Table 3. Structural Parameters of $Ca_4Mn_3O_{10}$ (Sample P) at 293 K

atom	site	*x*	*y*	*z*	U_{iso}/Å^2
Ca(1)	8c	0.5021(6)	0.4784(8)	0.06901(17)	0.0057(6)
Ca(2)	8c	−0.0024(9)	0.0167(12)	0.20399(12)	0.0094(8)
Mn(1)	4b	0	$^1/_2$	0	−0.0018(5)[a]
Mn(2)	8c	0.4961(9)	−0.0002(14)	0.14074(14)	−0.0018(5)[a]
O(1)	8c	0.4410(4)	0.0035(7)	0.06997(16)	0.0029(6)
O(2)	8c	0.5349(6)	−0.0059(9)	0.21082(9)	0.0013(6)
O(3)	8c	0.7853(7)	0.2139(8)	0.13265(10)	0.0078(7)
O(4)	8c	0.2159(6)	0.7824(7)	0.14696(9)	0.0051(6)
O(5)	8c	0.2885(7)	0.2886(8)	−0.00859(10)	0.0060(7)

[a] Constrained to be the same. Space group: *Pbca*. $a = 5.26557(12)$ Å, $b = 5.26039(11)$ Å, $c = 26.8276(5)$ Å, $V = 743.096(27)$ Å^3. Agreement indexes: $R_{wp} = 5.44\%$; $R_p = 4.21\%$; $R_f = 3.06$; $DWd = 0.45$; $\chi_{red}^2 = 5.78$ for 49 variables.

Table 4. Bond Distances (Å) and Angles (deg) for $Ca_4Mn_3O_{10}$ (Sample P) at 293 K[a]

Ca(1)−O(1)^{i}	2.781(6)	Ca(2)−Mn(2)	3.056(9)	Mn(1)−O(1)	1.903(4) × 2
Ca(1)−O(1)^{ii}	2.519(6)			Mn(1)−O(5)$^{i/iii}$	1.897(5) × 2
Ca(1)−O(1)^{iii}	2.337(4)			Mn(1)−O(5)$^{ii/iv}$	1.897(5) × 2
Ca(1)−O(1)^{iv}	2.935(4)	Ca(2)−O(2)^{i}	2.446(6)	Mn(2)−O(1)	1.921(6)
Ca(1)−O(3)^{i}	2.660(5)	Ca(2)−O(2)^{ii}	2.838(6)	Mn(2)−O(2)	1.891(5)
Ca(1)−O(3)^{ii}	2.388(5)	Ca(2)−O(2)^{iii}	2.524(8)	Mn(2)−O(3)	1.906(8)
Ca(1)−O(4)^{i}	3.034(5)	Ca(2)−O(2)^{iv}	2.761(8)	Mn(2)−O(3)	1.907(7)
Ca(1)−O(4)^{ii}	2.599(5)	Ca(2)−O(2)^{v}	2.297(3)	Mn(2)−O(4)	1.874(7)
Ca(1)−O(5)^{i}	2.568(5)	Ca(2)−O(3)^{i}	2.447(5)	Mn(2)−O(4)	1.867(7)
Ca(1)−O(5)^{ii}	3.056(5)	Ca(2)−O(3)^{ii}	2.902(6)		
Ca(1)−O(5)^{iii}	2.312(5)	Ca(2)−O(4)^{i}	2.276(5)		
Ca(1)−O(5)^{iv}	2.622(5)	Ca(2)−O(4)^{ii}	2.563(6)		

O(1)−Mn(1)-O(1)	179.97(1)	O(2)−Mn(2)-O(3)	92.1(3)
O(1)−Mn(1)-O(5)	89.1(1)	O(2)−Mn(2)-O(3)	92.0(3)
O(1)−Mn(1)-O(5)	89.7(1)	O(2)−Mn(2)-O(4)	89.3(3)
O(5)−Mn(1)-O(5)	89.10(5)	O(2)−Mn(2)-O(4)	89.3(3)
		O(3)−Mn(2)-O(3)	88.3(2)
O(1)−Mn(2)-O(2)	177.5(3)	O(3)−Mn(2)-O(4)	178.1(3)
O(1)−Mn(2)-O(3)	90.1(3)	O(3)−Mn(2)-O(4)	91.0(3)
O(1)−Mn(2)-O(3)	89.2(3)	O(3)−Mn(2)-O(4)	90.3(3)
O(1)−Mn(2)-O(4)	88.6(2)	O(3)−Mn(2)-O(4)	178.5(3)
O(1)−Mn(2)-O(4)	89.4(3)	O(4)−Mn(2)-O(4)	90.4(2)
Mn(1)−O(5)-Mn(1)	157.6(2)	Mn(2)−O(3)-Mn(2)	159.3(3)
Mn(1)−O(1)-Mn(2)	161.9(2)	Mn(2)−O(4)-Mn(2)	161.6(3)

[a] Superscripts relate to Figure 9.

lowering has been seen previously in $Sr_4Ti_3O_{10}$.[22] The refined structural parameters are listed in Table 1, and the observed and calculated diffraction patterns are plotted in Figure 1. Data analysis in this space group involved 24 atomic coordinates, 1 overall isotropic temperature factor, 4 peak shape parameters, and 12 background parameters. It was not possible to detect any deviation from the ideal oxygen content from these data. The derived bond lengths are listed in Table 2. The reduction in symmetry was also apparent in the neutron diffraction data collected on D2b, and refinement of the room-temperature crystal structure of sample P in *Pbca* resulted in the structural parameters listed in Table 3 and the bond lengths in Table 4. These refinements used eight isotropic thermal parameters, seven peak shape parameters, and six background parameters. The thermal parameter of the Mn cations took a small negative value, which may indicate the presence of uncorrected absorption effects. There was no significant improvement in the fit when the occupancies of the anion sites were allowed to vary. The resulting observed and calculated diffraction profiles are plotted in Figure 2, and the crystal structure is drawn in Figure 3. A section of the fitted profile is shown in Figure 4, together with the same region of the diffraction profile as collected on HRPD. It is clear from this

(22) Elcombe, M. M.; Kisi, E. H.; Hawkins, K. D.; White, T. J.; Goodman, P.; Matheson, S. *Acta Crystallogr.* **1991**, *B47*, 305.

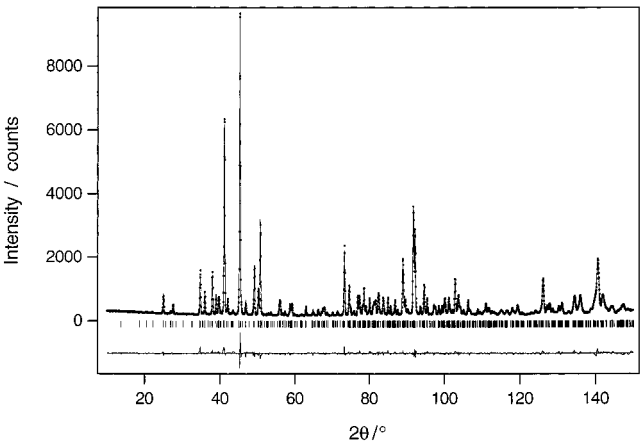

Figure 2. Observed (D2b), calculated and difference neutron diffraction profiles of $Ca_4Mn_3O_{10}$ (sample P, prepared under 1 atm of O_2) at room temperature. Reflection positions are marked.

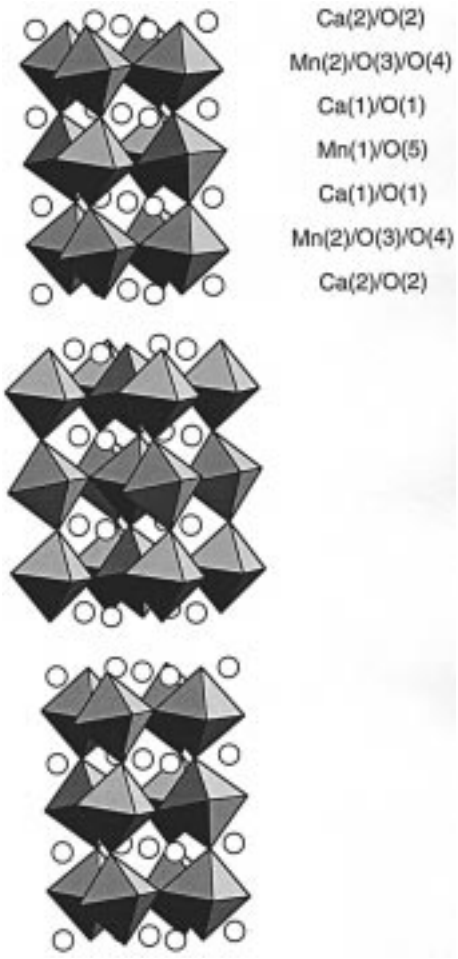

Figure 3. Crystal structure of $Ca_4Mn_3O_{10}$ (sample P) at room temperature.

figure that the concentration of defects in our sample is sufficiently high to cause anisotropic peak-broadening in the data collected on HRPD, which has an instrumental resolution $\Delta d/d \sim 8 \times 10^{-4}$, even though sample-dependent effects are not apparent in the lower-resolution D2b data ($\Delta d/d \sim 4 \times 10^{-3}$ for $d \sim 2$ Å). This result suggests that an investigation of the microstructure by electron microscopy would be valuable.

The molar magnetic susceptibility of sample P is plotted as a function of temperature in Figure 5 (the

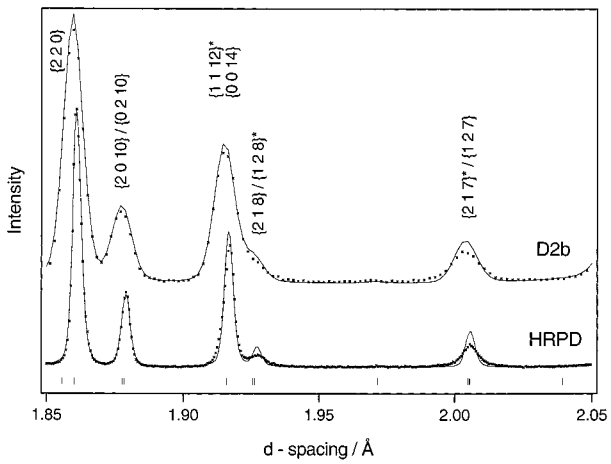

Figure 4. Comparison of peak broadening in the neutron diffraction profiles of $Ca_4Mn_3O_{10}$ (sample P) collected on D2b (upper) and HRPD (lower). Weak components of composite peaks are marked (with asterisks).

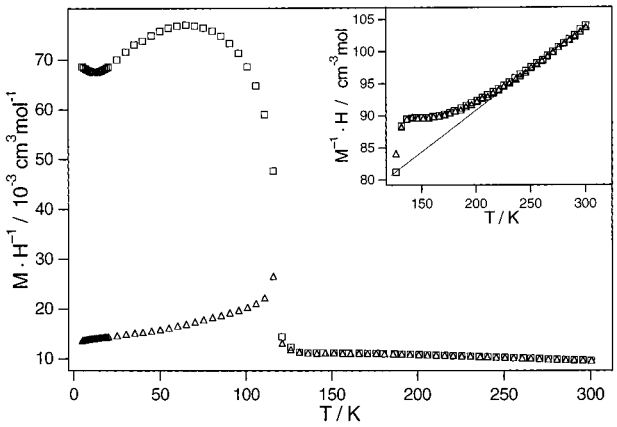

Figure 5. Molar magnetic susceptibility (M/H) of $Ca_4Mn_3O_{10}$ (sample P) as a function of temperature. The inset shows a Curie−Weiss fit for $T \geq 265$ K.

behavior of sample Q was qualitatively similar). Attempts to model the high-temperature region ($T \geq 265$ K) using a Curie−Weiss model resulted in nonsensical parameters ($\mu_{eff} = 4.54\ \mu_B$ per Mn, $\theta = -500$ K), and it is clear that interatomic magnetic interactions are significant throughout the measured temperature range. A magnetic phase transition occurs at 115 K, and the increase in the susceptibility below this temperature suggests that the sample acquires a spontaneous magnetization. However, the small magnitude of the magnetization at 5 K ($2 \times 10^{-3}\ \mu_B$ per Mn^{4+} in 500 G) suggests that the compound is not a classical ferromagnet but that it either contains small clusters of ferromagnetically aligned spins or it is a canted antiferromagnet. The additional Bragg scattering seen in the neutron diffraction data collected at 5 K (Figure 6) is consistent with the latter hypothesis. In view of the limited d-spacing range of these data, the atomic coordinates were held constant at their high-temperature values during analysis of the magnetic structure. The agreement between the observed and calculated intensities shown in Figure 6 was achieved using a model (Figure 7) in which G-type antiferromagnetic ordering[23] occurs within each perovskite block. In this

(23) Wollan, E. O.; Koehler, W. C. *Phys. Rev.* **1955**, *100*, 545.

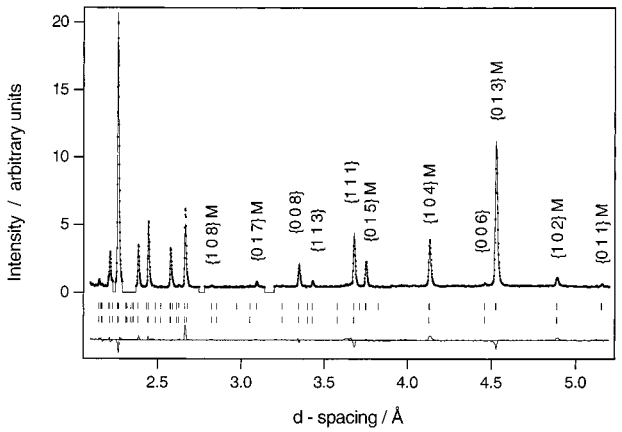

Figure 6. Observed, calculated, and difference neutron diffraction profiles for $Ca_4Mn_3O_{10}$ (sample P) at 5 K (IRIS). Upper (lower) reflection markers indicate the position of magnetic (nuclear) Bragg peaks. Regions of the profile containing peaks originating from the instrument were excluded from the refinement.

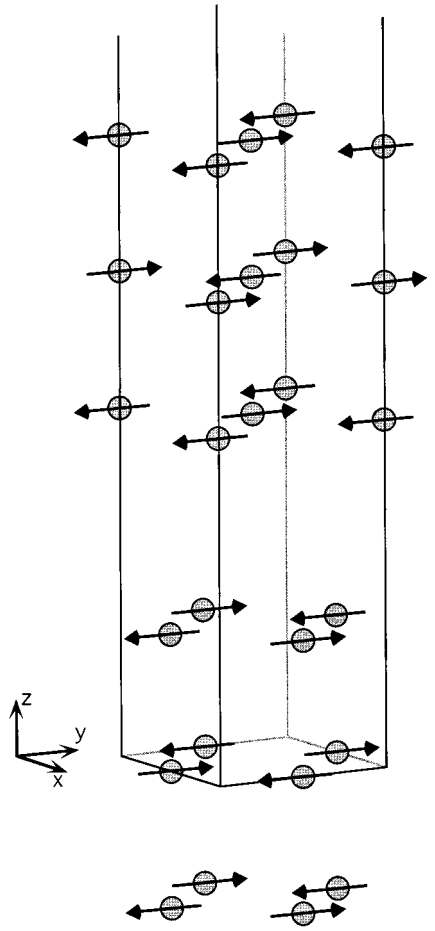

Figure 7. Magnetic structure of $Ca_4Mn_3O_{10}$ at 5 K; the spin directions of the Mn cations in two adjacent perovskite blocks are shown.

ordering scheme, each magnetic cation is coupled antiferromagnetically to its nearest-neighbors, six of them in the case of cations in the central layer of the block and five in the case of the cations in the outer layers. The resolution of our data was sufficient to show that the spins align along the *y* direction, with an ordered component of 2.23(2) μ_B per Mn. The interblock coupling is such that spins separated by a vector (0, $^1/_2$, $^1/_2$) are antiferromagnetically coupled. The weak ferromagnetic component of the magnetic structure is too small to be detected in our experiment. The unit-cell parameters of the magnetic phase refined to the following values: $a = 5.25353(7)$, $b = 5.25001(8)$, $c = 26.7660(5)$ Å.

Discussion

Our failure to achieve a reliable chemical analysis leaves some uncertainty over the precise oxygen content of our samples. However, refinement of the occupation fraction of the anion sites in sample P failed to detect any deviation from unity, thus indicating that the stoichiometry of this sample is very close to $Ca_4Mn_3O_{10}$. The unit-cell volume of sample P is slightly larger than that of sample Q, thus implying that the latter has a higher Mn^{4+} content and that the deviation from the formula $Ca_4Mn_3O_{10}$ is even less in this case. Both samples have smaller volumes than that reported for $Ca_4Mn_3O_{9.96}$,[19] which suggests that both are very close indeed to the composition $Ca_4Mn_3O_{10}$.

Our diffraction data show that the true crystal structure of both samples P and Q is an orthorhombic distortion of the idealized tetragonal form described originally.[19,24] Symmetry lowering was also observed in an electron diffraction study carried out by Rossell et al.,[25] although they assigned a space group (*Ccc*2, with $a = 5.240$, $b = 26.823$, $c = 5.276$ Å) which is incompatible with our observation of the {1 0 10} reflection at $d \sim 2.39$ Å. The unit-cell parameters, which show $a_Q < a_P$, $b_Q < b_P$, but $c_Q > c_P$, suggest that the use of high pressure has anisotropic consequences, but comparison of the data in Tables 1 and 3 shows that the compositional difference between samples P and Q is insufficient to cause any major structural variation, and we shall therefore base our discussion on the more precisely determined structure of sample P. The Mn(1)−O(1,5) bond lengths in the MnO_6 octahedra at the center of the perovskite blocks (Figure 8) are all essentially equal, and the O−Mn−O bond angles deviate from their ideal values by less than 1°. These octahedra can thus reasonably be described as regular. This is not true in the case of the octahedra on the edges of the blocks. The Mn(2)−O(2) bond, which is directed into the rock salt layer, is significantly shorter than the trans Mn(2)−O(1) bond, and the Mn(2)−O(3) bonds, which lie cis to each other within the layers, are equal to each other but longer than the trans Mn(2)−O(4) bonds. The bond angles in these octahedra also show larger deviations from 90 and 180° than those in the octahedra around Mn(1). However, the average Mn−O bond length (1.894 Å) around Mn(2) does not differ significantly from that around Mn(1) (1.899 Å), and both are shorter than the values measured in $n = 2$ RP phases containing mixed valence $Mn^{3.5+}$.[12,13,26] The extent to which the octahedra are tilted away from their ideal orientations can be seen from the Mn−O−Mn angles in Table 4 and the struc-

(24) Brisi, C.; Lucco-Borlera, M. *J. Inorg. Nucl. Chem.* **1965**, *27*, 2129.
(25) Rossell, H. J.; Goodman, P.; Bulcock, S.; March, R. H.; Kennedy, S. J.; White, T. J.; Lincoln, F. J.; Murray, K. S. *Aust. J. Chem.* **1996**, *49*, 205.
(26) Battle, P. D.; Millburn, J. E.; Rosseinsky, M. J.; Spring, L. E.; Vente, J. F. *Chem. Mater.* **1997**, *9*, 3136.

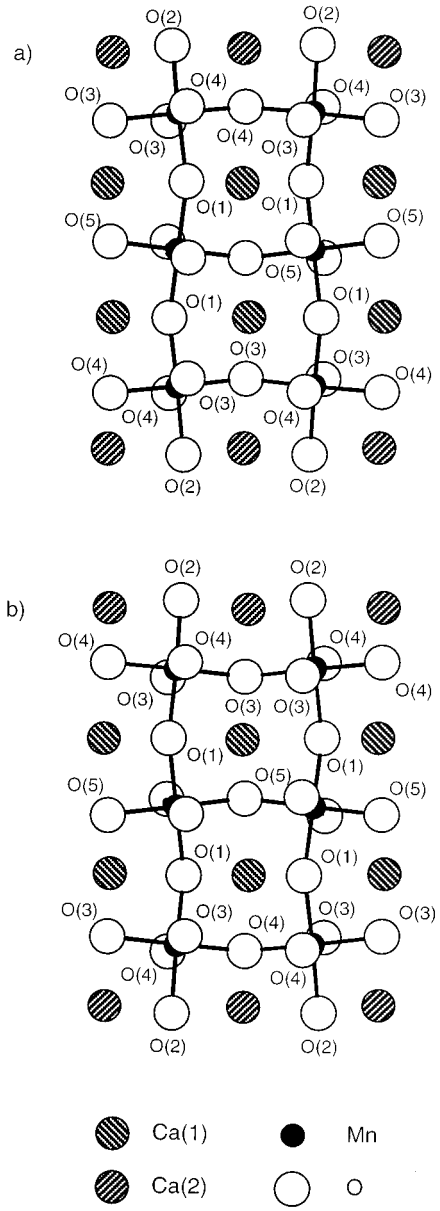

Figure 8. Tilting of MnO_6 octahedra viewed along directions close to (a) [1$\bar{1}$0] and (b) [1 1 0].

tural diagrams in Figures 3 and 8. The differences between the $Mn(1)O_6$ and $Mn(2)O_6$ octahedra described above do not have any parallel in the $n = 1$ and $n = 2$ phases, in which all the octahedra have the same environment by symmetry. The short Mn(2)−O(2) bond in $Ca_4Mn_3O_{10}$ should be contrasted with the equivalent bond in the $n = 2$ phases containing $Mn^{3.5+}$, which is always longer than the trans bond directed into the perovskite block. In the latter case, the partial occupation of the e_g orbitals plays an important role in determining the local coordination geometry, but this is not a factor in the Mn^{4+}:t_{2g}^3 compound. In the case of $Ca_4Mn_3O_{10}$, Mn(1) competes with Mn(2) for the electron density on O(1), whereas there is little competition for the electron density on O(2), and the Mn(2)−O(2) bond is consequently the shorter. The environment of the Ca cations (Figure 9) in the observed orthorhombic structure is also markedly different from that in the tetragonal structure originally proposed. Ca(1) in the perovskite blocks would be expected to have a coordination number of 12, but to achieve this value it is necessary to consider a shell of radius 3.056 Å, which is equal to the intercation Ca(2)−Mn(2) distance. Although the Ca(2) cations in the rock-salt layer have a wide range of bond distances to oxygen, they retain nine neighbors, which is the expected number for this site in an RP structure, within a shell of radius 2.902 Å. Interestingly, Ca(1) also has nine neighbors within a shell of radius 2.9 Å, and it can thus be argued that the tilting of the octahedra occurs to satisfy the coordination requirements of both of the inequivalent Ca^{2+} cations. The distortions in this $n = 3$ compound can be compared to those seen previously in the $n = 2$ RP phases $Sr_2HoMn_2O_7$ and $Sr_2YMn_2O_7$,[26] which retain tetragonal symmetry but show a rotation of the MnO_6 octahedra. However, in contrast to the $n = 3$ compound, in which the octahedra rotate about two perpendicular axes ([110] and [1$\bar{1}$ 0]) in the *xy* plane, the rotation in $Sr_2HoMn_2O_7$ and $Sr_2YMn_2O_7$ can be considered to occur about one axis only. Furthermore, the Sr cations within the perovskite blocks have 12 oxide ions within a distance of 2.9 Å. The increased distortion in the case of $Ca_4Mn_3O_{10}$ could be interpreted in terms of the change in the tolerance factor $(r_A + r_O)/\sqrt{2}(r_B + r_O)$ which occurs on passing from Sr to Ca and from $Mn^{3.5+}$ to Mn^{4+}.

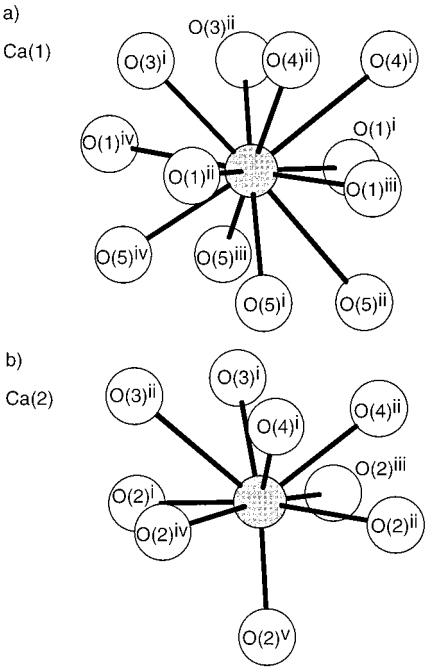

Figure 9. Coordination geometry around the cations Ca(1) and Ca(2) in $Ca_4Mn_3O_{10}$.

The magnetic susceptibility of sample P and the changes that occur in the neutron diffraction pattern between room temperature and 5 K strongly suggest that significant short-range magnetic interactions are operative at room temperature and that they cause a transition to a weakly ferromagnetic state (a canted antiferromagnet) on cooling below 115 K. This conclusion is consistent with that drawn by MacChesney et al.,[19] although they reported $T_N = 125$ K for $Ca_4Mn_3O_{9.96}$. It is likely that strong spin correlations exist within individual perovskite blocks at room temperature and that interblock interactions overcome thermal effects at the Curie temperature, which is only slightly lower than the magnetic ordering temperature of

$CaMnO_3$ (123 K[19]). Two-dimensional magnetic order has previously been reported to occur at relatively high temperatures in $n = 2$ phases[8]. The value of the antiferromagnetically ordered component of the Mn^{4+} magnetic moment measured by neutron diffraction is expected to be reduced from the ideal value ($3\mu_B$) by both covalency and zero-point spin deviation[27] effects, and it is also sensitive to orbital effects and errors in the form factor used to describe the angular dependence of the magnetic scattering factor. The errors introduced by ignoring the weak ferromagnetic component of the structure will be negligible in comparison. The moment measured using sample P ($2.23\mu_B$) is smaller than that measured[23] for $CaMnO_3$ ($2.6\mu_B$), which perhaps suggests that some residual spin disorder is present. However, the measured value lies in the expected range for a $3d^3$ cation coordinated by six oxygen atoms.[28] The spin arrangement in the antiferromagnetic phase is rather interesting, and the orthorhombic nature of the distorted structure must be considered in order to understand it. Each perovskite block has a G-type magnetic structure, with antiparallel alignment of the magnetic moments on nearest-neighbor cations. This ordering pattern occurs in a great many perovskites, including $CaMnO_3$, and is not remarkable in itself. It is, however, different from the ordering seen in $n = \infty$ $LaMnO_3$[29] and the $n = 2$ phases $Sr_2LaMn_2O_7$[13]and $Sr_2NdMn_2O_7$,[12] which show A-type magnetic ordering (ferromagnetic *xy* sheets with alternating spin directions along *z*) within the perovskite blocks. This implies that, in the fully oxidized $n = 3$ compound, the antiferromagnetic interactions between nearest-neighbor cations are strengthened relative to those between next-nearest neighbors. This is likely to be a result of the different electron configurations of Mn^{3+}:$3d^4$ and Mn^{4+}:$3d^3$, with the ferromagnetic interaction caused by the presence of an e_g electron in the former being absent when all the cations have a t_{2g}^3 configuration. The strengthening of the antiferromagnetic interaction between nearest neighbors on moving from the $n = 2$ compounds to $Ca_4Mn_3O_{10}$ is thus due to the loss of the competing ferromagnetic component. However, variations in cation size and acidity should not be completely ignored when discussing changes in the strengths of superexchange interactions. The consequences of this change in magnetic structure for the magnetotransport properties will be discussed in a subsequent publication. In the ideal tetragonal structure there would be two degenerate ways of coupling the spins in one block to those in the neighboring block along *z*, for example (Figure 7) the spin at (0, $^1/_2$, 0.14) will interact antiferromagnetically with that at ($^1/_2$, $^1/_2$, 0.36) and with that at (0, 0, 0.36), and one of these interactions would be frustrated in an antiferromagnetic tetragonal structure. However, the orthorhombic distortion removes this degeneracy, and the antiferromagnetic superexchange along the shorter ($b < a$) pathway dominates.

In conclusion, we have shown that, for small values of δ, $Ca_4Mn_3O_{10-\delta}$ adopts an orthorhombic $n = 3$ Ruddlesden−Popper structure with a pronounced tilting of the MnO_6 octahedra being caused by the coordination requirements of the Ca^{2+} cations. The observation of a spontaneous magnetization below 115 K encourages us to believe that this phase may show interesting magnetotransport properties, although the underlying antiferromagnetic structure differs from that adopted by $n = 2$ and $n = \infty$ GMR manganates. Experiments to investigate this possibility are in progress.

Acknowledgment. We would like to thank the Royal Society (an equipment grant to M.J.R.), Departamento de Educacion, Universidades e Investigacion, Gobierno Vasco−Eusko Jaurlaritza (J.L.), EPSRC (M.A.G. and J.F.V.) and the donors of the Petroleum Research Foundation, funded by the American Chemical Society (J.E.M.) for financial support. We also thank A. R. Pennell, Dr. P. G. Radaelli (ILL), Dr. R. M. Ibberson (RAL) and the magnetotransport group in the Clarendon Laboratory, University of Oxford, for experimental assistance and stimulating discussions.

CM970647R

(27) Tofield, B. C.; Fender, B. E. F. *J. Phys. Chem. Solids* **1970**, *31*, 2741.
(28) Battle, P. D.; Macklin, W. J. *J. Solid State Chem.* **1984**, *52*, 138.
(29) Koehler, W. C.; Wollan, E. O. *J. Phys. Chem. Solids* **1957**, *2*, 100.